J. Ind. Geophys. Union (October 2010)
Vol.14, No.4, pp.219-232

Assessment of diurnal urban surface temperature and impervious surface of Delhi and its relationship using Multi-Spectral satellite data

Yogesh Kant, Javed Mallick[1] and Atiqur Rahman[1]
Indian Institute of Remote Sensing (NRSC), ISRO, Govt. of India, Dehradun - 248 001
[1]Department of Geography,Jamia Millia Islamia, New Delhi
E.mail : ykanty@yahoo.com, yogesh@iirs.gov.in

ABSTRACT

Satellite data is used to assess the urban land cover and its thermal characteristics through mapping sub-pixel impervious surface and assessing thermal infrared images. The study aims to calculate urban imperviousness using linear spectral unmixing technique. ASTER dataset were used to estimate land surface temperature (day and night time) over National Capital Delhi using the surface emissivity information at pixel level. The result suggests that the methodology is feasible to estimate NDVI, surface emissivity and surface temperature (with an error of 3 degree) with reasonable accuracy over heterogeneous urban area. Spatial and diurnal distribution of surface temperature associated with ISA (impervious surface area) is studied. The lower imperviousness has low night time surface temperature because of the predominance of non-imperviousness (such as vegetation, soil, pasture lands etc). In contrast, the higher ISA coverage associated with high-density urban areas such as high-density residential, commercial and industrial possessed higher imperviousness values. The relationship between day and night time surface temperature with impervious surface indicated that night time surface temperature has a strong positive correlation (0.82) with impervious index as compared to day time temperature. The results suggests that night time surface temperature gives more information in understanding UHI phenomena than day time due to radiative cooling differences are maximized between urban and surrounding rural locations at night.

INTRODUCTION

In urbanization process removal of pervious (natural land cover) land cover types such as water, soil, and vegetation and their replacement with impervious materials such as concrete, asphalt, stone, brick and metals have significant environmental implication. This leads to reduction in evapotranspiration, promotion of more rapid surface runoff, increase storage and transfer of sensible heat and reduction of air and water quality. The result of this change can have significant effects on local weather and climate (Landsberg 1981). The interactions of urban land surfaces with the atmosphere are governed by surface heat fluxes, the distribution of which is significantly modified by urbanization.

Impervious surface is a key indicator of urban environmental quality and degree of urbanization (Weng 2007). The estimation and mapping of urban impervious surface by using satellite images has paid lot of attention to the researches. Impervious surfaces can lead to severe environmental problems and are recognized as an important indicator of environmental quality (Arnold & Gibbons 1996). The increase in imperviousness surface can lead to increase the volume of surface runoffs (Weng 2001). Impervious surfaces can also disrupt the recharge of underground water and increase the frequency of flooding (Brun & Band 2000). Because impervious surfaces replace the natural vegetation, and other biophysical variable, they can cause environmental degradation and negative effects on atmospheric carbon cycling. Moreover, impervious surfaces are strongly associated with urban heat Islands (UHIs) (Weng et al., 2006).

Significant research has performed in using remotely sensed information to detect thermal characteristics of urban surfaces. Some studies used measurements of temperature using temperature sensors mounted on car, along various routes (Yamashita 1996). These methods are both expensive and time consuming and lead to problems in spatial interpolation. Satellite borne instruments can provide quantitative physical data at high spatial, temporal resolutions with repetitive coverage and capability of measurements of earth surface conditions (Owen et al., 1998). Voogt & Oke (2003) reviewed the use of thermal remote sensing for the study of urban climates with respect to the heat islands and described the distinction between the atmospheric and the surface UHIs. The use of satellite infrared remote sensing in estimating the surface physical properties and variables has been investigated e.g. Carlson et al., (1981), Balling & Brazel (1988), Dousset (1989, 1991), Roth *et al*., (1989), Quattrochi & Ridd (1994), Owen *et al*., (1998), Voogt & Oke (1998), Lo & Quattrochi (2003); Dousset & Gourmelon (2003). Luke Howard, a pioneer in urban climatology, first measured temperature differences across London as early as 1809 (Chandler 1968). But our understanding of urban effects on local climate is still unsatisfactory due to several difficulties: 1) the inherent complexity of the city-atmosphere system, 2) lack of a clear conceptual theoretical framework for inquiry, and 3) the high expense and enormous difficulties of acquiring a sufficient quantity of high-quality, high-resolution (both spatially and temporally) observations in cities.

This paper presents a methodology that is based on emissivity factor and correction of atmospheric effect for estimating the urban surface temperature and UHI intensity of urban areas using ASTER thermal images and estimation of impervious surface using linear spectral unmixing technique. Various image masks were developed by using land use/land cover and water bodies (including river beds) and applying them to linear spectral mixing analysis (LSMA) — derived impervious surface image in order to improve the accuracy of impervious surface mapping. The study also evaluates statistically the relationship between day-time, night-time surface temperature with impervious surface.

STUDY AREA

The capital city of India, New Delhi is geographically situated between latitude 28° 23' 17'' to 28° 53' 00'' North and Longitude 76° 50' 24'' to 77° 20' 37'' East lies at an altitude between 213 and 305 m and covers an area of 1,483 km^2. It is situated on the bank of river Yamuna and is bordered in the east by the state of Uttar Pradesh and on the north, west, and south by the state of Haryana. The climate of Delhi is influenced by its remote inland position and prevalence of air of continental character, which is characterised by extreme summer heat in June (48 ^{0}C), alternating with severe winter cold December (3 ^{0}C). Only during the three monsoon months of July-September, oceanic air penetrates the country deep to the Northern region. The climate of Delhi is of semi-arid nature due to marked diurnal differences in temperature, high saturation deficit and low/ moderate annual average rainfall (60 mm). The desert area of Rajasthan is to the west, south-west and the Gangetic plains of Uttar Pradesh to the east, across which the monsoon air travels and reaches Delhi, have their respective shares in affecting the climate of this region. Extreme dryness with an intense hot summer and cold winter are the features, which are associated with sweep of air from westerly or north-westerly direction, while the influx of air from the easterly or south-easterly directions usually causes increased humidity, cloudiness and precipitation. The urban population of Delhi increased at 3.87% annual growth rate during 1991-2001. The latter is influenced by the gradual shifting of the rural area and its merger with urban area. With the continuation of the present population trend, the total population of National Capital Territory (NCT) Delhi by the year 2011 and 2021 would be 18.2 million and 22.5 million respectively. As per Census 2001, NCT Delhi had a population of 13.78 million and 46.28 percent decennial population growth during 1991-2001.

METHODOLOGY

Image Pre-Processing

Satellite datasets of Terra ASTER level-1B (Level 1-B product contains radiometrically calibrated and geometrically co-registered data for all ASTER channels) over Delhi area of October 07, 2001 (night time) of path/row 13/204 and October 18, 2001 (day time) of path/row 146/40 have been used for estimation and mapping of impervious surfaces using linear spectral unmixing and estimation of surface temperature. DN values were converted to at sensor radiance, for ASTER using L_λ = (DN-1) X UCC

UCC is unit conversion coefficients from HDF file. The unit conversion coefficients that are used for different bands and for different gain settings are given in ASTER User Handbook. ASTER level-1B was geometrically corrected data sets. For standardization, ASTER 15 m data (VNIR) and Landsat -7 ETM+ Panchromatic data (15 m resolution) both were compared to each other and was noticed that geometrical accuracy was low. Also the GPS readings in the ground did not match with these locations. Hence there was a need to further rectify and standardize all the datasets. All the image were geometrically rectified to a common Universal Transverse Mercator (UTM) WGS84 coordinate system and were resampled to its spatial resolution using the nearest- neighborhood algorithm.

After applying the radiometric and geometric corrections, the subset images of radiance were created for the study area, both for visible and near infrared bands of the ASTER datasets. Standard atmospheric and geometric parameters were estimated using the ENVI FLAASH (Fast line-of-sight atmospheric analysis of spectral hypercubes) software. The FLAASH models include a method for retrieving an estimated aerosol/haze amount from selected "dark" land pixels in the scene (Kaufman et al., 1997). These parameters along with the geometric parameters for each of the images were used together for atmospheric correction.

The following land use/ land cover classification scheme has been adopted:

High dense built-up, low dense built-up, commercial /industrial area, dense vegetation (forest), sparse vegetation (including parks), water bodies, fallow land, waste land/bare soil and agricultural cropland.

A total of nine land use/land cover classes were considered to represent the major LU/LC of the study area. An extensive field visit had been conducted during October 3-8, 2005 for ground truth collection. Sample points were selected, so as to cover all the major LU/LC classes in the area. Also measurements pertaining to emissivity and surface temperature on various LU/LC feature were taken using the emissivity box and infrared thermometer.

ESTIMATION OF IMPERVIOUS SURFACE USING LINEAR SPECTRAL MIXTURE ANALYSIS (LSMA)

To characterize and study at sub-pixel level of impervious surface, linear spectral mixture approach (SMA) is used. The linear SMA approach assumes that the spectrum measured by a sensor is a linear combination of the spectra of all the components within the pixel (Weng & Schubring 2004). The mathematical model of linear SMA can be expressed as,

$$R_i = \sum_{k=1}^{n} f_k R_{ik} + \varepsilon_i \qquad (1)$$

Where,
i = the number of spectral bands used
$k = 1,....,n$ (Number of endmembers)
R_i = the spectral reflectance of band i of a pixel, which contains one or more endmembers
f_k = the proportion of endmember k within the pixel
R_{ik} = known as the spectral reflectance of endmember k within the pixel on band i
And ε_i is the error for band i

To solve f_k, the following conditions must be satisfied

- Selected endmembers should be independent of each other
- The number of endmembers should be less than or equal to the spectral bands used
- Selected spectral bands should not be highly correlated

Estimation of an endmember fraction image with linear SMA involves the following steps: (i) image processing; (ii) endmember selection and (iii) unmixing solution and evaluation of fraction image. Of the above steps, selecting of suitable endmember is the most critical to achieve a high quality fraction image (Weng & Schubring 2004). Two types of endmembers can be applied, such as image endmembers, and reference endmember. Image based endmembers are preferred because they can be easily obtained from the image feature space and no calibration is needed between selected endmembers and the spectra measured. This method uses high-resolution digital imagery (IKONOS) to develop training data for representing urban land cover heterogeneity, and medium-resolution ASTER imagery to extrapolate impervious surface area (ISA) over large regions. Prior to derivation of the fraction image, the Minimum Noise Fraction (MNF) transformation was performed. Three types of endmembers were selected: vegetation, soil and built-up (concrete and asphalt). Vegetation was selected from the areas of dense vegetation and dense grassland. Different types of impervious surface from image were selected from buildings roofs, airport runways, highways intersection etc. Soils were selected from bare ground surface. These endmembers were compared with those selected from image scatter plots (using MNF components). The endmembers with similar MNF components spectra located at the extreme vertices of the scatter plots were finally selected.

The information on vegetation and soils should not be contained in the impervious images. Hence image masks were developed based on land use/land cover and water bodies (including river beds) in order to improve the accuracy of impervious surface mapping

Estimation of surface temperature using temperature emissivity separation (TES) algorithm

Temperature Emissivity Separation (TES) algorithm was applied to Terra-ASTER datasets for estimation of surface temperature. TES attempts to compensate for reflected downwelling irradiance and estimates the absolute spectral emissivity. The additional constraint to overcome the under-determination comes from the regression of the minimum emissivity of spectral contrast (calculated from laboratory spectra), used to equalize the number of unknowns and measurements, so that the set of Planck's equations for the measured thermal radiances can be inverted. ASTER has 14 spectral bands, out of which 5 thermal bands 10-14 operate between 8-12 μm. In this study, five emissivity and one surface temperature maps were produced using the TES algorithm. It not only estimates the temperature of homogeneous areas of known emissivity, such as water bodies, but also for heterogeneous areas of unknown emissivity. The spectral radiance of thermal bands at the sensor is calculated using the following equation (Gillespie *et al.*, 1998)

$$LS_j = [\varepsilon_j L^{BB}{}_j(T) + (1-\varepsilon_j)L_j^{sky}] \times \tau_j + L_j^{atm} \quad (2)$$

Where,
LS_j = spectral radiance observed by the sensor,
ε_j = surface emissivity at wavelength j,
$L^{BB}{}_j(T)$ = spectral radiance from a blackbody at surface temperature T,
L_j^{sky} = spectral radiance incident upon the surface from the atmosphere (downwelling), from MODTRAN,
L_j^{atm} = spectral radiance emitted by the atmosphere (upwelling), from MODTRAN
τ_j = spectral atmospheric transmission, from MODTRAN.

The pixels are often mixed in vegetation regions, which complicates the measurement of mean pixel emissivity. In this study, the Normalized Difference Vegetation Index (NDVI) information of each pixel in conjunction with proportional vegetation cover was used to approximate the mean pixel emissivity (Kant & Badarinath 2000).

The at-sensor radiance data were corrected for atmospheric effects to obtain the radiance emitted by the surface (L_j), using the MODTRAN radiative transfer model. The standard atmospheric parameter (tropical climate) has been considered. The retrieved output parameters were used to estimate the radiance using following equation:

$$L_j = [LS_j - L_j^{atm} \div \tau_j] - (1-\varepsilon_j)L_j^{sky} = \varepsilon_j L^{BB}{}_j(T) \quad (3)$$

Where, $L^{BB}{}_j(T) = \dfrac{C_1}{\lambda_j^5[\exp(C_2/\lambda_j T) - 1]}$

Hence, $$L_j = \varepsilon_j \times \frac{C_1}{\lambda_j^5[\exp(C_2/\lambda_j T) - 1]} \quad (4)$$

where,
C_1 = First radiation constant = 3.74151×10^{-16}
C_2 = First radiation constant = 0.0143879 (mk)
λ_j = Wavelength of channel j,
T= Temperature

In the above equation, if the surface emissivity is known, it is possible to correct for the reflected sky radiation. The surface temperature then can be calculated using

$$T_j = \frac{C_2}{\lambda 1n}[(\varepsilon_j C_1 / L_\lambda \lambda^5 \pi) + 1] \quad (5)$$

The above equation shows that for radiance measured in 'n' spectral channels, there will be 'n+1' unknowns, 'n' emissivities and one surface temperature. In TES (Gillespie *et al.*, 1998; Schmugge *et al.*, 1998) the estimated kinetic temperature is taken to be the maximum temperature, estimated from the radiance for the five ASTER TIR spectral bands, computed from equation (5), and using an assumed emissivity value (typically 0.97) in order to be within ± 0.03 for typical land surfaces (heterogeneous lands). The relative emissivities ('B_j') were computed by the following equations:

$$\beta_j = (L_j / \overline{L_j}) \times (\overline{L^{BB}} / L^{BB}(\lambda_j, T)) \quad (6)$$

where,

$$\overline{L_j} = (1/5)\sum_{j=1}^{j=5} L_j \quad (7)$$

$$L^{BB}{}_j(T) = \frac{C_1}{\lambda_j^5[\exp(C_2/\lambda_j T) - 1]} \quad (8)$$

$$\overline{L^{BB}(T)} = (1/5)\sum_{j=1}^{j=5} L_j^{BB}(T) \quad (9)$$

For emissivities between 0.7 – 1.0, the ratios B_j are generally within 0.7 – 1.4.

The maximum-minimum difference between the emissivity ratios is given by MMD = max (B_j) - min (B_j). It was observed that MMD ranges from 0.0 to 4.0 at most. An empirical relation between minimum emissivity and MMD is:

$$\varepsilon_{\min} = 0.994 - 0.687 \times (MMD)^{0.737} \quad (10)$$

Therefore, the revised emissivity can be computed using the beta (B_j) spectrum as shown below:

$$\varepsilon_j = \beta_j (\varepsilon_{\min} / \min(\beta_j)) \quad (11)$$

Beta (β_j) is determined from the measured surface radiance (surface); new emissivity (ε_j) and surface temperature can be obtained. The resultant maps were fed into equation (2) and all the process until

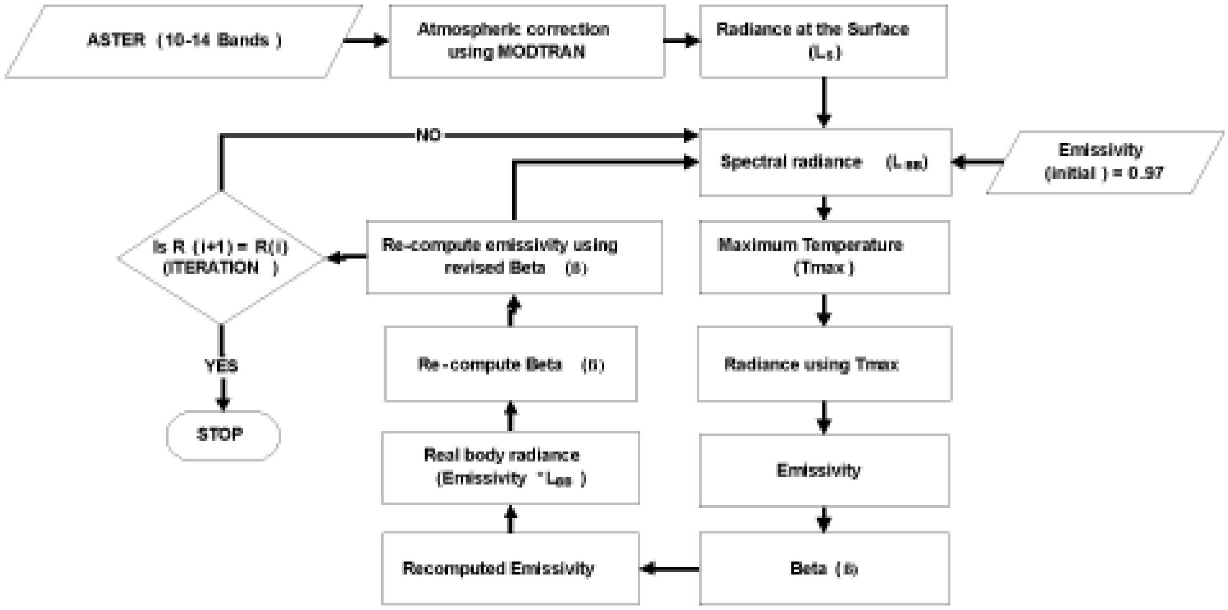

Figure 1. Flow Chart for deriving surface temperature (TES) using ASTER data.

equation (11) where repeated so as to arrive at an acceptable emissivity measurement, which is further used. Based on the above procedure, a detailed model was developed in the ERDAS Imagine to automate the calculation of the surface temperature and five emissivity maps (as the TES algorithm generate). Figure 1 shows the methodology adopted for estimating surface temperature using TES algorithm.

RESULTS AND DISCUSSION

Analysis of impervious surface estimation

Figure 2 shows the spatial distribution of impervious surface estimation using LSMA of ASTER, dated October 18, 2001. The fraction cover (FC) values are estimated in range of 0 to 1, having a mean value of 0.452 and standard deviation of 0.103. High fraction covers of impervious surface (red areas) are observed in the eastern, central and south-east region of the image. Low fraction cover values are observed mostly in suburb central region. Overall, the fraction image shows the spatial pattern and abundance of each surface material (used in endmembers). However fraction cover features namely water and shade areas are problematic for estimation of impervious surface. To reduce the impact of non-impervious surface, image masks (LULC together with water/river beds) are applied to the original impervious surface to refine the results.

Analysis of Surface Emissivity

An attempt has also been made in this study to measure the emissivity using the emissivity box (Kant & Badarinath 2002). All the measurements of temperature were done using TELATEMP infrared radiometer which operates in the 8-14 µm waveband with an instantaneous field of view (IFOV) of 2^0 with an accuracy of 0.1 ^{0} C. The measurements were made using Emissivity box during October 4 to 7, 2005 at various places taking different features of interest on all sunny days at different hours of the day. This is achieved in the field by exposing the hot lid to direct solar radiation for 15 minutes so that the thermal equilibrium can be attained. To reduce the effect of noise in the final result, the value is taken after averaging over 10-15 successive measurements. The emissivity values presented here are the results of *in situ* measurements in and around Delhi area. The measurements could not be done on all the sample features of the area but only carried out over some selected (dominant) features representing that LU/LC class. The measurements were carried on soil (for wasteland/bare soil), dense vegetation (Prosopis *juliflora*, Bougainvillea in forest), sparse vegetation (grass, Azadirachta indica A. Jurr), agricultural crop (paddy), and urban (concrete, asphalt roads and sandstone). To determine the sample emissivity, the hot lid temperature must be higher than the sample temperature (15-20 ^{0} C) and remain constant during

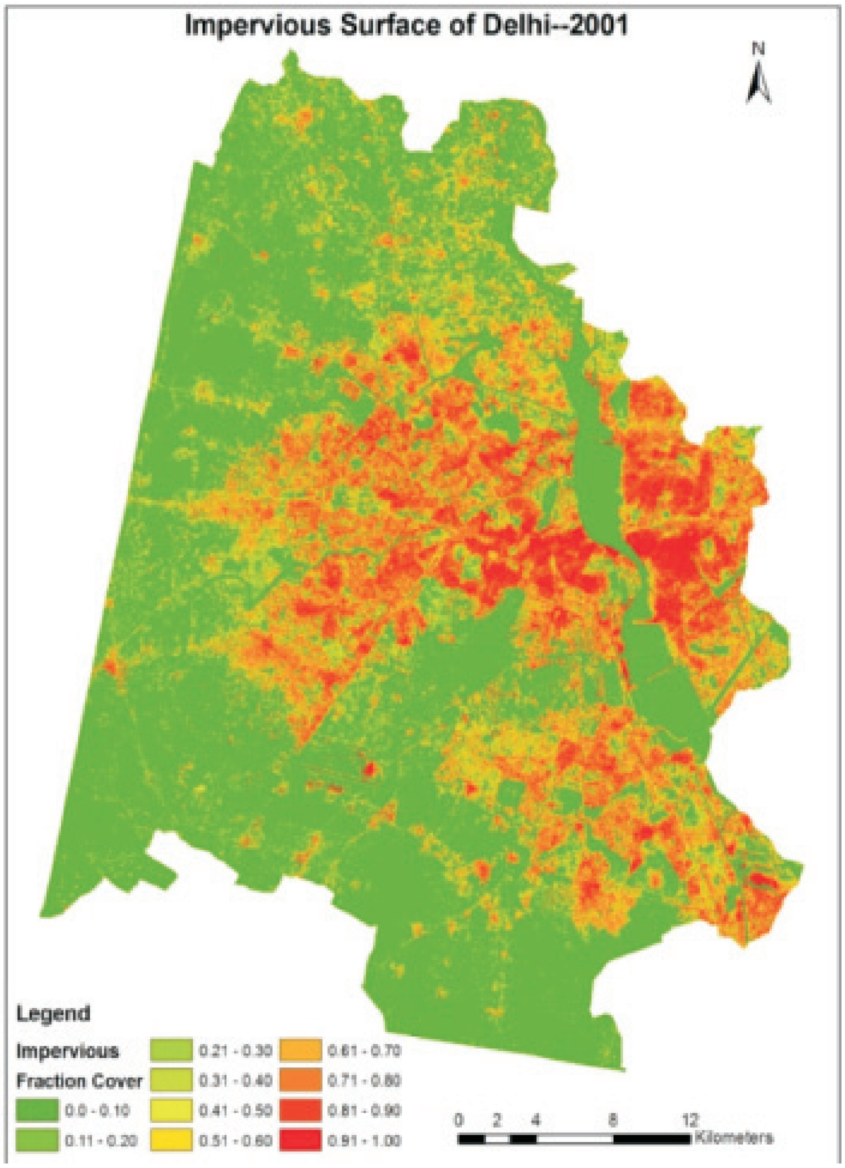

Figure 2. Spatial distribution of impervious surface Fraction cover estimation using LSMA (ASTER, October 18, 2001).

the time necessary for making L^1 and L^2 measurements. The emissivity measurement is rapidly made (within 2 minutes) in order that the temperature variation of the hot lid can be negligible when it is introduced in the box. The emissivity measurement was carried out during the middle of the sunny day when the stability of the system is greater. The value of the emissivities measured over soil and vegetation by the box method using the radiometer is shown in table 1. It can be concluded that there is not much variation in emissivity values neither through the day nor between the clear days of the period. Hence, the average of the measurements can be taken as the values of the respective samples. The mean can be considered as a representative value that can be used in practice whereas standard deviations show the variability in emissivity values. The measured emissivity values were compared with those measured by Owe & Griend 1994 in Botswana campaign (tropical area) for bare soil in 8-14 μm region (ε =0.914) which agrees well with the measured value over soil (ε = 0.923) and open grass (partly covered) (ε = 0.949) with the measured value over grass in parks (ε = 0.9668).

Table 1. Field measurements of emissivity in the 8-14 μm band for different samples.

Date	Soil	Sparse vegetation	Dense Vegetation	Urban (concrete)	Agricultural cropland (Paddy)
October 4, 2005	0.923 $\pm$ 0.013	0.9560 $\pm$ 0.015	-	0.9156 $\pm$ 0.012	-
October 5, 2005	-	-	0.9810 $\pm$ 0.006	-	0.9850 $\pm$ 0.013
October 6, 2005	-	0.9775 $\pm$ 0.016	0.9807 $\pm$ 0.012	0.9378 $\pm$ 0.014	-
MEAN	**0.923 $\pm$ 0.013**	**0.9668 $\pm$ 0.015**	**0.9808 $\pm$ 0.09**	**0.9267 $\pm$ 0.013**	**0.9850 $\pm$ 0.013**

ANALYSIS OF SURFACE TEMPERATURE

The surface temperature is estimated for ASTER datasets (day time –October 18, 2001) and night time (October 7, 2001). The spatial distribution of surface temperature of ASTER, dated October 18, 2001 at 11:18 hrs (local time) is shown in figure 3(a). It is inferred that the estimated land surface temperature ranges from 24.35 °C to 54.29°C (mean value of 37.83°C with standard deviation of 4.235). It is also observed that, west and south-west part of the image exhibits maximum surface temperature due to fallow land and waste land/bare soil; surface temperature in eastern part ranges from 36 to 40°C and in the range of 32 to 36°C in central part of the image. water bodies exhibit lowest surface temperature values (ranges from 27.96 to 32.86°C). Over vegetated areas, agricultural cropland has lowest values (ranges from 28.93 to 32.94°C) as compared to dense vegetation and sparse vegetation (ranges from 29.57 to 35.02°C). This may be due to the fact that the surface temperature (crop temperature) is in equilibrium with air temperature. In urban areas, commercial/industrial land use (ranges from 35.17 to 43.93°C) has high surface temperature values than low dense and high built-up. This may be due to the commercial/industrial activities compounded with the building structures. The highest surface temperatures are observed over fallow lands (ranges from 41.16 to 53.09°C).

Figure 3(b) shows the night time surface temperature of ASTER night time data (October 7, 2001) at 22:35 hrs local time. The estimated surface temperature ranges from 23.90 to 40.01°C (mean value of 31.40°C and standard deviation of 1.863). It is inferred that central and eastern part of the image exhibits maximum surface temperature range (32 to 36°C) that corresponds to built-up areas. It is observed that some parts of north-west have lower surface temperature corresponding to wasteland/bare soil and fallow land. Water bodies exhibits maximum surface temperature during night due to high thermal capacity.

The day and night time mean thermal gradient of surface temperature over different land use/ land cover for the two Aster datasets is depicted in figure 4. The thermal gradient during day time increases from water bodies to fallow land, whereas in the night time, mean thermal gradient decreases from high dense built-up to fallow land. In the surface temperature statistics of night time data the highest surface temperature is observed over high dense built-up, followed by water bodies, commercial/industrial and low dense built-up. Fallow land and waste land/ bare soil due to low thermal capacity cools down faster than other land use/land cover features. Hence fallow land, waste land/bare soil and sparse vegetation are cooler as compared to other land use/land cover features during night time.

Figure 5 shows the spatial distribution of surface temperature over impervious surface of Delhi (aforesaid LU/LC mask applied to impervious surface). An image masks have been applied to the surface temperature images (day time–night time) in order to understand the relationship with impervious surface.

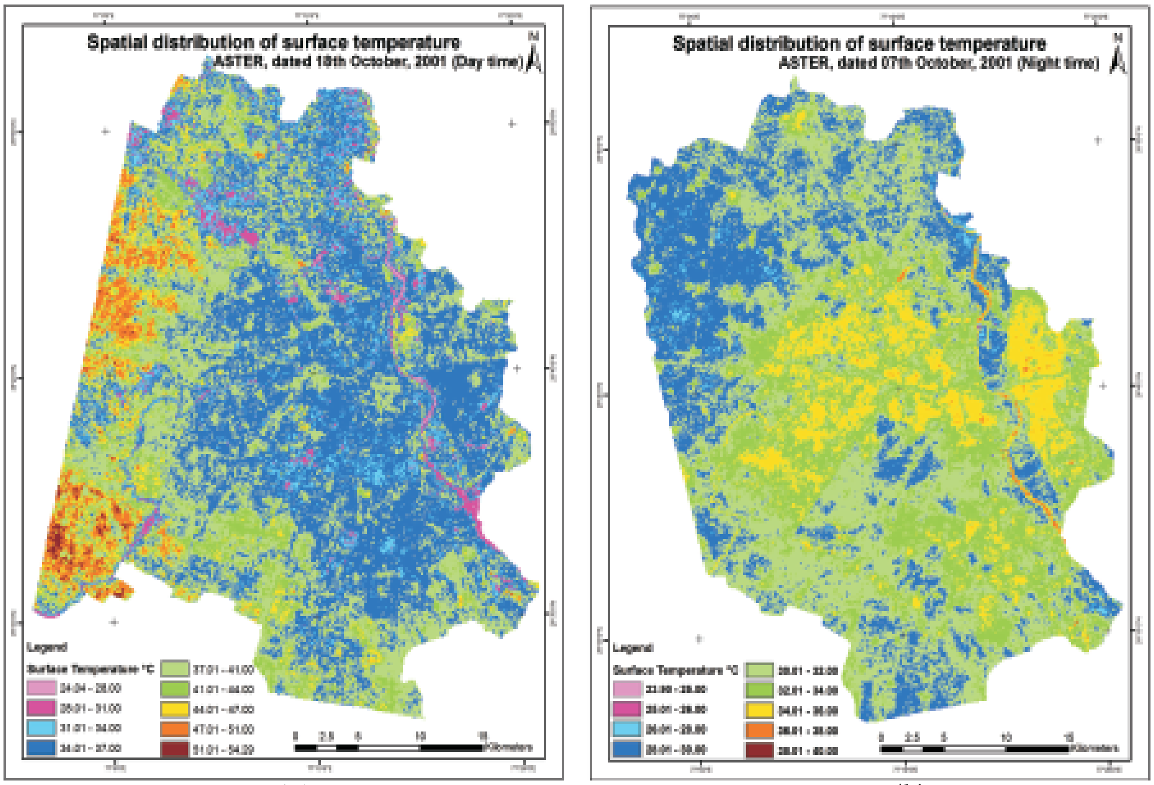

(a) (b)

Figure 3. Spatial distribution of surface temperature of Delhi (a) ASTER data of October 18, 2001 (day time) and (b) ASTER data of October 7, 2001 (night time).

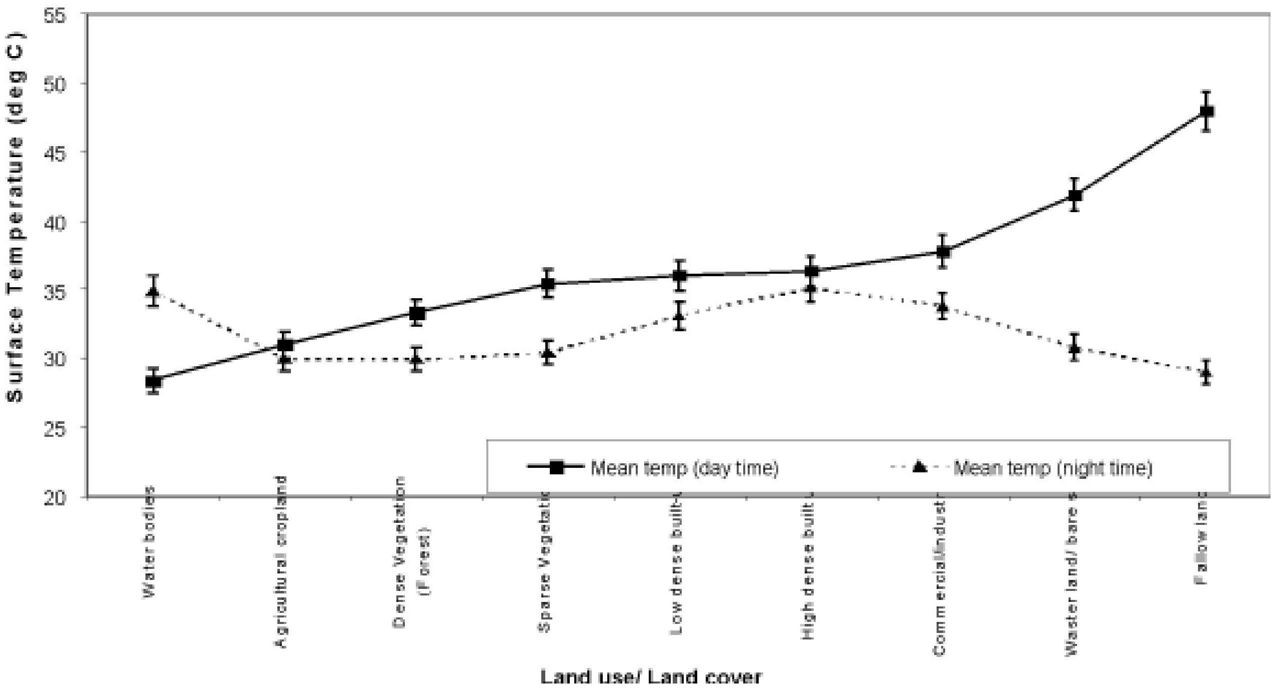

Figure 4. Surface temperature over different Land use/ land cover features over Delhi.

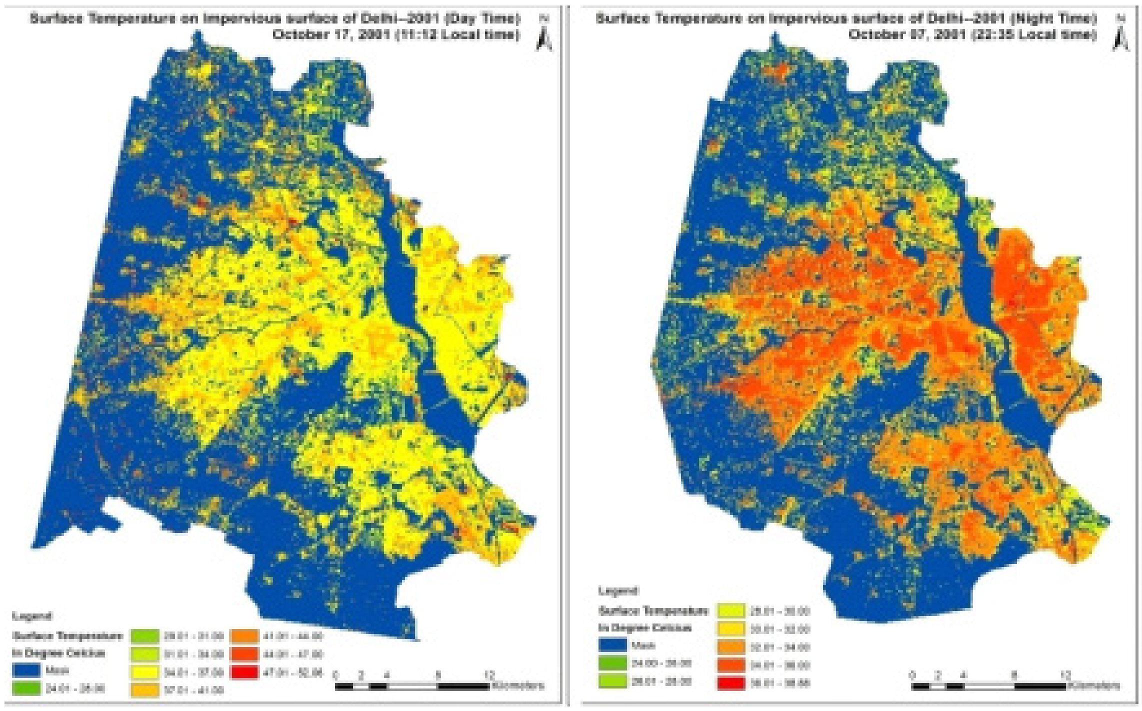

(a) (b)

Figure 5. Spatial distribution of surface temperature over impervious surface of Delhi (a) ASTER data of October 18, 2001 (day time) and (b) ASTER data of October 7, 2001 (night time).

COMPARISON OF OBSERVED AND ESTIMATED SURFACE TEMPERATURE

All the satellite datasets taken for this study is for the month of October. In order to compare the satellite estimated surface temperature values with the field measurements, a field campaign from October 2 -7, 2005 was carried out. All the measurement of temperature were done using TELETEMP infrared radiometer which operates in the 8-14 μm waveband with an instantaneous field of view (IFOV) of 2^o with an accuracy of 0.1^oC. During the campaign surface temperature measurements were taken during day and night time over different features. In the absence of field measurement in year 2001, the estimated surface temperature values have been compared with those of the year 2005, maintaining the same period of season. Table 2 shows the comparison of day and night time surface temperature values from observed field data with estimated satellite derived surface temperature. The satellite (ASTER night time, dated October 7, 2001) derived surface temperature are found to be in close agreement with the ground measured values with errors within $\pm$ 3^0 C. To find out the difference between the temperatures on October 7, 2001 and October 7, 2005 ambient air temperature measurement were collected from India Meteorological Department (IMD) at Sufdarjung monitoring station, Delhi. The maximum and minimum temperature on October 7, 2001 were 34.8°C and 22.8°C, while on October 7, 2005 were 34.6°C and 21.5°C respectively which were appreciably close. The comparison of field measured surface temperature values with night time ASTER data October 7, 2001 reveals that the error in surface temperature estimation is within range of $\pm$ 3°C.

Relationship between impervious surface and diurnal land surface temperature

This section deals with the relationship between day and night time surface temperatures and impervious surface. The Pearson's correlation coefficients were computed between surface temperatures with fraction cover for imperviousness. Imperviousness values ranges from 0 to 1 (mean value of 0.388 and standard deviation of 0.241), indicating the surface covered by building roofs, roads, airport runways and pavements abundance. The mean surface temperature for each imperviousness category is taken into account. Table 3 shows the Pearson's correlation between day and night time surface temperature with impervious surface cover, for the entire image. During night time it is inferred that surface temperature has a strong positive correlation with impervious index while during day time surface temperature has a low

Table 2. Comparison of satellite derived night time surface temperature with field measurement.

Features	*In the field, observation on October 7, 2005 in °C		Satellite observation (ASTER October 7, 2001)		UTM Coordinates
	(10.30 to 12.00 Hrs local time)	(21.30 to 23.00 Hrs local time)	Day time (10.35 IST) in °C	Night time (22.35 IST) in °C	
Dense Vegetation	33.20	28.50	32.58	29.64	718935 / 3159479
Dense Vegetation	34.52	28.00	32.36	28.95	717613 / 3160398
Sparse Vegetation	36.25	29.00	33.59	30.25	719570 / 3169243
Sparse Vegetation	36.45	29.30	33.88	30.67	718365 / 3167032
Average	**35.11**	**28.70**	**33.10**	**29.88**	-
Bare soil	46.15	28.50	49.52	30.88	700395 / 3158756
Bare soil	47.25	30.42	50.13	31.03	701456 / 3162141
Average	**46.70**	**28.33**	**49.83**	**30.95**	-
Concrete (Low dense built-up)	34.60	31.10	37.32	32.90	719871 / 3168740
Concrete (High dense built-up)	35.80	31.65	38.79	33.72	717812/3169034
Average	**35.20**	**31.38**	**38.14**	**33.31**	-

***This measurement is the mean value of 5 to 10 readings**

Table 3. Pearson's correlation between surface temperature (day time, dated 18th October 2001and night time, dated 07th October 2001) with impervious surface cover of ASTER (at resolution of 90 meter).

Night time	**ST**	**Impervious surface**
ST (surface temperature) Night time	1.000	0.816**
Impervious surface Fraction cover	0.816**	1.000
Day time	**ST**	**Impervious surface**
ST (surface temperature) Day time	1.000	0.159**
Impervious surface Fraction cover	0.159**	1.000

** Correlation is significant at the 0.01 level (1-tailed)

correlation. This may be due to the impact of soil and vegetation portion (fraction cover) that has low thermal capacity. While at night, radiative cooling differences are maximum between urban and surrounding rural locations and high imperviousness reveals high thermal capacity than lower impervious surface. Hence night time surface temperature data reveals good correlation with imperviousness.

The graphical representation of linear regression coefficient between surface temperature and impervious surface is depicted in figure 6. Regression coefficient between surface temperature with imperviousness is found to be high at night time (0.810) and low (0.159) during day time. It is noticed

Table 4. Statistical values of surface temperature over each imperviousness category.

Imperviousness surface (fraction)	Mean Ts (night time) in ^{0}C	S.D	Mean Ts (day time) in ^{0}C	S.D
0.001 - 0.10	31.440	1.565	35.058	9.718
0.11 -0.20	31.482	1.535	34.604	9.783
0.21 - 0.30	31.692	1.555	35.255	8.364
0.31 - 0.40	31.949	1.579	35.565	7.292
0.41 - 0.50	32.220	1.628	35.398	7.198
0.51 - 0.60	32.421	1.617	35.777	6.155
0.61 - 0.70	32.622	1.619	35.929	5.459
0.71 - 0.80	33.077	1.574	36.104	4.242
0.81 - 0.90	33.250	1.528	35.992	4.366
0.91 - 1.00	33.524	1.486	36.172	3.580

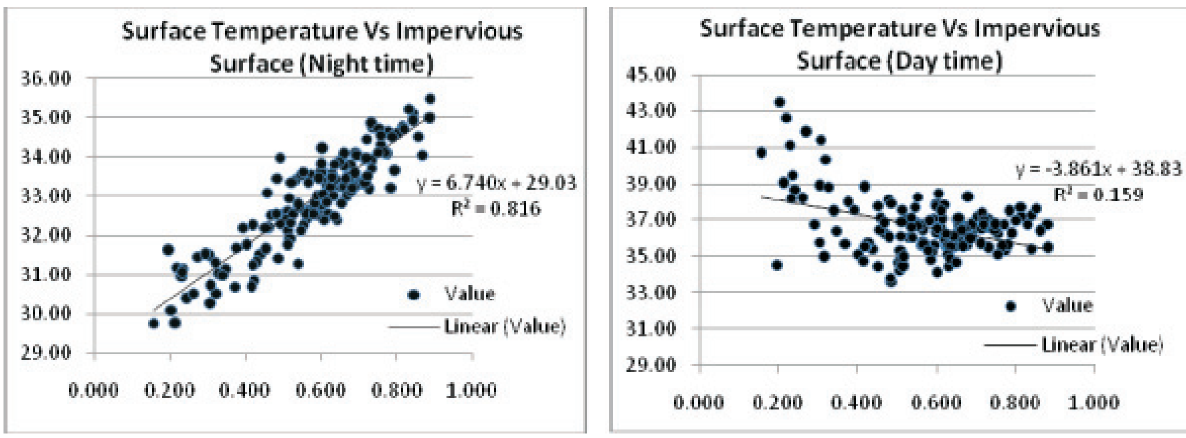

Figure 6. Linear regression coefficient between surface temperature and impervious surface.

that at night time, magnitude of imperviousness lead to increases in surface temperature. The mean surface temperature (day and night time) over impervious surface categories is given in table 4. It is inferred that an increase in imperviousness also enhances the surface temperature. Hence, conversion of natural surface with urban concrete structure leads to an increases in surface temperature and in turn effect the local climate of the city. Low imperviousness has low surface temperature due to the predominance of non-imperviousness features (such as vegetation, soil, pasture lands etc). In contrast, the higher ISA coverage associated with high-density urban areas such as high-density residential, commercial and industrial land possessed higher imperviousness values.

CONCLUSIONS

Urban development intensity and spatial extent can be characterized by using satellite remote sensing data through mapping the impervious surface distributions. The diurnal temperature patterns over the impervious surface have been studied. It is concluded that during day time the most dominant surface elements contributing heat are building roofs, streets and artificial pavements that are exposed to solar radiation and there is no evaporative cooling effect over these surfaces. Moreover, impervious surface generate long wave radiation than non-impervious surface. As a result, not only do large asphalt and concrete paved surfaces have high temperatures but they are also expected to influence the temperatures of the near-surface air layer. The overall behaviour of night time surface temperature over impervious surfaces reveals that the temperatures are high in comparison to non-impervious surfaces. Low imperviousness fraction has low night time surface temperature because of the predominance of non-imperviousness (such as vegetation, soil, pasture lands etc.). In contrast, the higher ISA (Impervious Surface Area) coverage associated with high-density urban areas such as high-dense residential, commercial and industrial land possessed higher imperviousness values. During night time it is found that surface temperature has strong positive correlation with impervious index than during day time mainly due to cumulative impact of soil (fraction cover) which attributes low thermal capacity. Hence, it is concluded that understanding UHI phenomena using night time surface temperature is better and is more informative than day time as during night radiative cooling differences are maximum between urban and surrounding rural locations.

REFERENCES

Arnold, C.L. & Gibbons, C.J., 1996. Impervious surface coverage: the emergence of a key environmental indicator, J. of the American Planning Association., 62, 243–258.

Balling, R.C. & Brazel,S.W., 1988. High- resolution surface temperature patterns in a complex urban terrain, Photogrammetric Engineering and Remote Sensing., 54(9), 1289-1293.

Brun, S.E. & Band, L.E., 2000. Simulating runoff behaviour in an urbanizing watershed. Computer, Environment and Urban Systems., 24, 5–22.

Carlson, T.N., Dodd, J.K., Benjamin, S.G., & Cooper, J.N., 1981. Satellite estimation of the surface-energy balance, moisture availability and thermal inertia, J.of Applied Meteorology., 20 (1), 67-87.

Chandler, T.J., 1968. Urban climates. Proceedings of the Symposium on Urban Climates and Building Climatology, Brussels, October 1968, World Meteorological Organization, Technical Note 1 (108).

Dousset, B., 1989. AVHRR-derived cloudiness and surface temperature patterns over the Los Angeles area and their relationships to land-use, Proc. IGARSS-89, Vancouver, BC, Canada, IEEE., 2132–2137.

Dousset, B., 1991.Surface temperature statistics over Los Angeles: the influence of land use," in Proceedings of IGARSS-91, I.E.E.E., 367-371

Dousset B. & Gourmelon, F., 2003. Satellite multi-sensor data analysis of urban surface temperatures and landcover, ISPRS J. of Photogrammetry and Remote Sensing., 58 (1-2), 43-54.

Gillespie, A., Shuichi Rokugawa, Tsuneo Matsunaga, J., Steven Cothern, Simon Hook, & Anne B. Kahle, 1998. A temperature and emissivity separation algorithm for Advanced Space borne Thermal Emission and Reflection Radiometer (ASTER) images, IEEE Transactions on Geosciences and Remote Sensing., 36 (4), 1113-1126.

Kant, Y & Badarinath, K.V.S., 2002. Ground based method for measuring thermal infrared effective emissivities: Implications and perpesctives on the measurement of land surface temperature from satellite data, Int. J. of Remote Sensing., 23(11), 2179- 2191.

Kant, Y & Badarinath, K.V.S., 2000. Studies on land surface temperature over heterogeneous areas using AVHRR data, Int. J.of Remote Sensing., 21 (8),1749-1756.

Kaufmann, Y.J., Wald, A.E., Remer, L.A., Gao, B.C., Li, R.R. & Flynn, L., 1997. The MODIS 2. mm Channel-Correlation with visible reflectance for use in remote sensing of aerosol, IEEE Transactions on Geo-science and Remote Sensing., 35, 1286-1298.

Landsberg, H.E., 1981. The urban climate, New York: Academic Press.

Lo, C.P. & Quattrochi,D.A., 2003. Land- use and land-cover change, urban heat island phenomenon, and health implications: A remote sensing approach, Photogrammetric Engineering and Remote Sensing., 69(9), 1053-1063.

Owe, M., & Van de Griend., 1994. Ground based measurement on surface temperature and thermal emissivity, Advances in Space Research., 14, 45-58.

Owen, T.W., Carlson, T.N., & Gillies, R.R.., 1998. Remotely sensed surface parameters governing urban climate change, Int. J. of Remote Sensing., 19,.1663–1681.

Quattrochi, D.A., & Ridd, M.K., 1994. Measurement and Analysis of thermal energy responses from discrete urban surfaces using remote sensing data, Int. J. of Remote Sensing., 15 (10), 1991-2022.

Roth, M., Oke, T. R. & Emery, W. J., 1989. Satellite-derived urban heat islands from three coastal cities and the utilization of such data in urban climatology, Int. J. of Remote Sensing., 10, 1699-1720.

Schmugge, T., Hook, S.J. & Coll, C., 1998. Recovering Surface Temperature and Emissivity from Thermal Infrared Multi spectral Data, Remote Sensing of Environment., 65, 121- 131.

Voogt, J.A. & Oke, T.R.,1998. Effects of urban surface geometry on remotely-sensed surface temperature, Int. J. of Remote Sensing., 19, 895-920.

Voogt, J.A. & Oke, T.R., 2003. Thermal remote sensing of urban climates, Remote Sensing of Environment., 86

(3), 370–384.

Weng, Q., 2001. Modeling urban growth effect on surface runoff with the integration of remote sensing and GIS, Environmental Management., 28, 737–748.

Weng, Q., Lu, D. & Schubring, J., 2004. Estimation of land surface temperature-vegetation abundance relationship for urban heat island studies, Remote Sensing of Environment., 89, 467-483.

Weng, Q., Lu, D. & Liang, B., 2006. Urban surface biophysical descriptors and land surface temperature variations, Photogrammetric Engineering and Remote Sensing, 72, 1275–1286.

Weng, Q., 2007. Remote sensing of impervious surfaces: an overview, In Remote Sensing of Impervious Surfaces, Q. Weng (Ed.), pp. xv–xxvii (Boca Raton, FL: CRC/Taylor & Francis).

Yamashita, 1996. Detail Structure of Heat Island Phenomena from Moving Observations from Electric Trans Cars in Metropolitan Tokyo, Atmospheric Environment., 30, 429 435.

(Revised accepted 2010 September, 28; Received 2010 February 19)

Dr. Yogesh Kant holds doctorate in Physics from Osmania University, Hyderabad in 2000. He obtained his Master's degree in Physics from HNB Garhwal University in 1995. Presently, he is working as Scientist in Indian Institute of Remote Sensing (NRSC), Dehradun. His research field pertains to Remote sensing application to land surface processes, environmental physics. He has developed algorithms for extraction of geo-physical parameters using satellite data, participated in BIBEX, INDOEX field campaigns related to gas emission and aerosols and has experience in collecting data from ground based instruments. Published over 50 research papers in various national and international Journals, he was conferred IGBP START Young Scientist award in the year 2002. He is a member of IGU, ISRS, IASTA and visited Japan, Syria, Singapore and The Netherlands to attend conferences and scientific meetings.

Dr. Javed Mallick holds a doctorate in Geography, specialization in Urban Geoinformation from Jamia Millia Islamia (Central University), India in 2010. He obtained his Master of Science degree in Geography from Jamia Millia Islamia, India in 2001 and also earned Master of Science degree with specialization in Geoinformatics from International Institute for Geoinformation Science and Earth Observation (ITC), The Netherlands. He worked as a Research Associate with TERI (The Energy and Resources Institute), New Delhi India. He also worked in Atheeb Intergraph Saudi Company as GIS specialist, Riyadh, Kingdom of Saudi Arab. The main current directions of his research work are Urban Environmental Dynamics—Micro climate effects; Mapping art development for characterization of biophysical features such as emissivity, surface temperature; Application of RS/GIS in cadastral mapping using DGPS survey; Geo-telecommunication—Integration with OSP/ISP; Biodiversity Characterization and Assessment; and Arial Photography processing i.e. Arial Triangulation (AT), DEM generation, Orthophoto etc. He has a number of research paper publications to his credit both in international and national journals.

Dr. Atiqur Rahman is Associate Professor at the Department of Geography, Jamia Millia Islamia, Delhi, India. His area of interest is on Urban Environmental Management Issues, Remote Sensing & GIS. He was Post Doctoral Fellow at UFZ-Centre for Environmental Research, Leipzig, Germany (1998). He worked as Co-PI (1999-2000) Indo-German (DST-DAAD) joint research project. He was a member of Scientific Research Team of NASA funded UEM project (2004-2007) on Urban Ecology and Sustainability. He is the recipient of prestigious Young Scientist Project by the Department of Science and Technology, Govt. of India (2001-2004). Dr Rahman is the Member of Steering Committee (SC) of Population and Environment Research Network (PERN). Recently he has been awarded a major research project (2009-2012) by the Ministry of Environment & Forest, Govt. of India. He has a number of research publications to his credit both in international and national journals. He has widely traveled around the globe to attend conferences and scientific meetings.